ABUAD Journal of Engineering Research and Development (AJERD)
ISSN (online): 2645-2685; ISSN (print): 2756-6811

Volume 8, Issue 2, 259-267

Effect of Heat Treatment on Microstructure, Acidic Corrosion Resistance and Wear Performance of Low-Carbon Steel

Basiru Philip ARAMIDE[1, 2], Tamba JAMIRU[2], Taoreed Adesola ADEGBOLA[2], Abimbola Patricia Idowu POPOOLA[3]

[1]*Department of Agricultural and Environmental Engineering, Obafemi Awolowo University, Ife, Nigeria*
abashiruphilip@gmail.com

[2]*Department of Mechanical and Mechatronic Engineering, Tshwane University of Technology, Pretoria, South Africa*
AramideBP@tut.ac.za/JamiruT@tut.ac.za/AdesolaAT@tut.ac.za

[3]*Department of Chemical, Metallurgy and Materials Engineering, Tshwane University of Technology, Pretoria, South Africa*
PopoolaAPI@tut.ac.za

Corresponding Author: abashiruphilip@gmail.com, +2347020742576
Date Submitted: 04/06/2025
Date Accepted: 13/07/2025
Date Published: 31/07/2025

Abstract: *Low-carbon steels are widely used in structural and industrial applications, but their performance can be significantly enhanced through controlled thermal processing. This paper looks at how different heat treatment techniques affect low-carbon steel's microstructure, corrosion resistance in acidic settings, and wear performance. Mechanical and electrochemical behaviours were evaluated under four heat treatment conditions: normalizing (A), water quenching (Q), normalizing followed by quenching (AQ), and double (cyclic) quenching (QQ). Phase changes were characterized by optical microscopy; Vickers microhardness testing and depth profiling evaluated hardness distribution. Using linear polarization techniques, electrochemical corrosion tests in dilute sulfuric acid (H_2SO_4) were run to find corrosion potential, current density, and polarization resistance. Using a pin-on-disc apparatus, wear performance was also assessed under 10 N and 20 N loads. Results revealed that quenching greatly increased surface hardness because of martensite formation; Q had the highest microhardness but lower corrosion resistance because of microstructural stress and heterogeneity. By contrast, AQ offered a balanced microstructure with fair hardness and excellent corrosion resistance. Wear rates were closely connected to hardness; QQ showed the greatest wear resistance at both load conditions. These results highlight* the importance of heat treatment in maximizing the surface integrity of carbon steel for uses in mechanically hostile and acidic environments.

Keywords: *Heat Treatment, Low-Carbon Steel, Acidic Corrosion Resistance, Wear Behavior, Microstructure Evolution*.

1. INTRODUCTION

Its low cost, simplicity of manufacture, and good mechanical qualities make carbon steel one of the most often used engineering materials. Particularly in settings that need intermediate strength and formability, it is widely used in the construction, transportation, and energy sectors [1, 2]. Carbon steel's adaptability allows it to be customized for particular uses by means of heat treatment techniques, alloying, and surface changes. Though usually need protective coatings or certain grades to improve its longevity, carbon steel struggles in corrosive settings despite its great prevalence [3-6]. Focusing on creating advanced grades with improved strength-to-weight ratios and corrosion resistance, ongoing material science research is still enhancing carbon steel's qualities [7, 8]. Still, in some sectors, the use of carbon steel can be limited by its vulnerability to corrosion in particular settings. Different surface treatments and coatings have been created to improve the corrosion resistance of the material without sacrificing its preferred qualities in order to solve this problem [9-12].

Furthermore, continuous study aims at maximizing the microstructure and composition of carbon steel to enhance its performance in rigorous applications. Beyond its mechanical qualities, carbon steel's adaptability includes the ability to be customized to fit particular needs via heat treatment techniques [13]. Processes like quenching and tempering let one precisely regulate the microstructure of the material, hence producing a great variety of strength and toughness combinations. For several sectors, including automotive, construction, and energy, carbon steel is desirable because of its adaptability [14, 15]. Advances in manufacturing methods have in recent years produced high-strength low-alloy (HSLA) steels, which provide better mechanical qualities and corrosion resistance over conventional carbon steels. These materials incorporate trace quantities of alloying elements such as niobium, vanadium, and titanium to improve performance without substantially raising production costs [16].

Environmental concerns and sustainability are become increasingly significant, which has also influenced the carbon steel industry. The carbon footprint linked with steel making is being reduced by improved energy efficiency, more use of recycled materials, and the exploration of alternative manufacturing processes [17, 18]. Research on the creation of more robust and corrosion-resistant carbon steel grades also seeks to increase the life of steel products, hence supporting sustainability objectives.

Carbon steel is still a key component in many applications as the need for high-performance materials keeps increasing. From everyday household goods to vital infrastructure components, its capacity to be readily machined, welded, and shaped into complex forms makes it perfect for a broad spectrum of products [19, 20]. The continuous research and development in carbon steel technology promises to further increase its applications and capacities in the future.

The improvement of heat treatment parameters to improve carbon steel performance is the main focus of this study. This work intends to obtain best combinations of strength, toughness, and other desirable qualities by means of precise adjustment of the heat treatment process, hence increasing the possible uses of carbon steel in many sectors. The results of this study will support the continuous work to increase the adaptability and efficiency of carbon steel, therefore complementing the objectives of the sector of sustainability and improved material performance.

2. MATERIALS AND METHODS

This research endeavor investigated the influence of diverse heat treatment methodologies on the corrosion resistance and wear characteristics of low-carbon steel subjected to an acidic environment. The steel composition comprised 0.45% carbon, in conjunction with minimal quantities of aluminum (0.17%), silicon (0.12%), and manganese (1.32%), with iron constituting the principal element. Specimens were fabricated as 5 mm-thick rectangular plates to guarantee homogeneity.

Heat treatment was executed utilizing an electric muffle furnace, incorporating four separate protocols: normalizing (A), wherein specimens were elevated to 750°C and subsequently cooled in ambient air to promote ferrite–pearlite formation; water quenching (Q), characterized by heating to 750°C followed by rapid cooling in water to facilitate martensitic transformation; normalizing succeeded by quenching (AQ), where samples were initially air-cooled and subsequently reheated to 1000°C before quenching to realize a balance of toughness and hardness; and double (cyclic) quenching (QQ), which involved two consecutive quenching cycles at 750°C and 1000°C to augment structural uniformity. Subsequent to the treatment, the samples were sectioned employing a precision wire-cutting apparatus, followed by grinding and polishing utilizing silicon carbide (SiC) abrasives (10–30 µm), and further refined with monocrystalline diamond suspensions (1 µm and 9 µm) to attain a smooth, reflective surface. A 2% Nital solution was utilized for metallographic etching. Optical microscopy (Nikon OPM, 5× to 100×) was employed to analyze the microstructure and ascertain phases such as ferrite, pearlite, and martensite.

Corrosion testing was conducted in a dilute sulfuric acid (H_2SO_4) solution utilizing an AUTOLAB potentiostat configured in a standard three-electrode arrangement. Linear polarization resistance (LPR) methodology was employed to evaluate the corrosion potential (ECORR), corrosion current density (ICORR), polarization resistance (RP), and corrosion rate. The wear behavior was assessed utilizing a pin-on-disc apparatus under two distinct loads, 10 N and 20 N, applied over a duration of 30 minutes of sliding at ambient temperature. Weight loss was quantified to ascertain wear rates, and the worn surfaces were subjected to microscopic scrutiny. Microhardness testing was conducted using the Vickers method with a 300 g load and a 15-second dwell duration, with average values derived from twenty indentations per sample. An untreated control group was incorporated to facilitate comparative analysis with the four heat-treated cohorts. This comprehensive methodology provided the framework for correlating heat treatment with microstructural evolution, electrochemical degradation in acidic environments, surface hardness, and wear resistance.

3. RESULTS AND DISCUSSION

3.1 Microstructural Analysis by Optical Microscopy

The optical micrographs in Figures 1 to 4 illustrate the surface morphology and phase distribution of carbon steel specimens subjected to different heat treatment conditions: normalizing (A), water quenching (Q), normalizing followed by quenching (AQ), and cyclic quenching (QQ). The temperature histories and transformation mechanisms are directly evident in the reported variations in grain structure, phase clarity, and homogeneity.

The micrographs of Sample A exhibit a typical ferrite-pearlite microstructure characterized by relatively coarse, equiaxed grains. The mild phase contrast at 50× magnification (Figure 1a) signifies a reduced cooling rate that allowed for a near-equilibrium transition. At 100× magnification (Figure 1b), the ferrite regions exhibit a lamellar morphology, interspersed with lighter areas and darker pearlite clusters. This structure, characterized by ductile and softer steel, has moderate strength and excellent formability, making it suitable for applications necessitating impact resistance.

The microstructure of Sample Q is significantly more refined than that of the air-cooled sample. The 100× image (Figure 2b) demonstrates a complete martensitic transition induced by rapid quenching, exhibiting acicular or needle-like martensitic features. The 50× image (Figure 2a) displays a densely packed grain structure. The contrast between bright and dark appears to be more uniform, indicating reduced ferrite retention. The elevated hardness values seen in this sample, along with the uniformity and refinement of the martensitic laths, indicate significant hardness and strength, but with diminished flexibility. The AQ sample has a heterogeneous microstructure, signifying a partial martensitic transition within a ferrite-pearlite matrix. At 50× (Figure 3a), the structure appears more refined than A but less consistent than Q. At 100× (Figure 3b), black martensitic patches are apparent adjacent to lighter, finer ferritic areas, indicating incomplete transition

resulting from previous air cooling. This dual-phase structure provides a balance between hardness and toughness, advantageous in applications necessitating wear resistance while maintaining ductility.

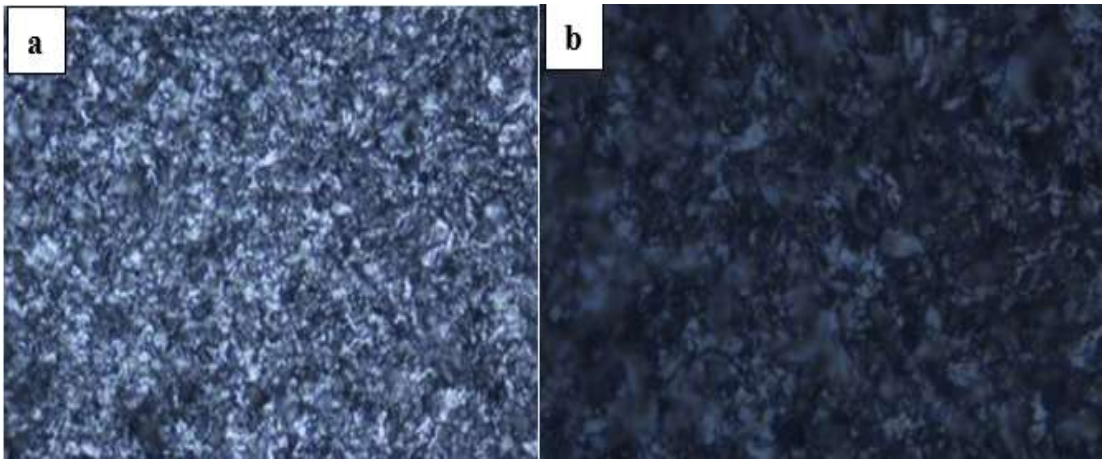

4

Figure 1: The OPM micrograph for sample A: a) 50x Magnification, b) 100x Magnification

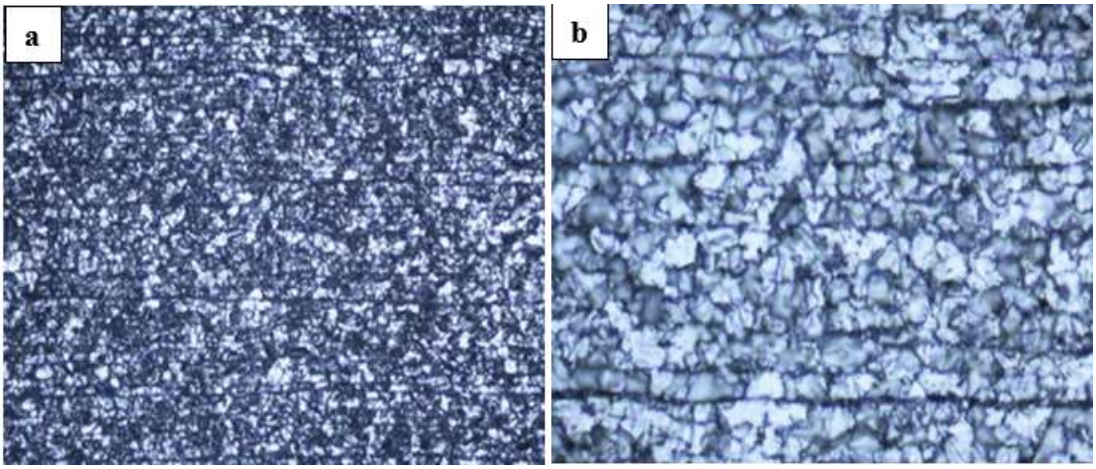

Figure 2: The OPM micrograph for sample Q: a) 50x Magnification, b) 100x Magnification

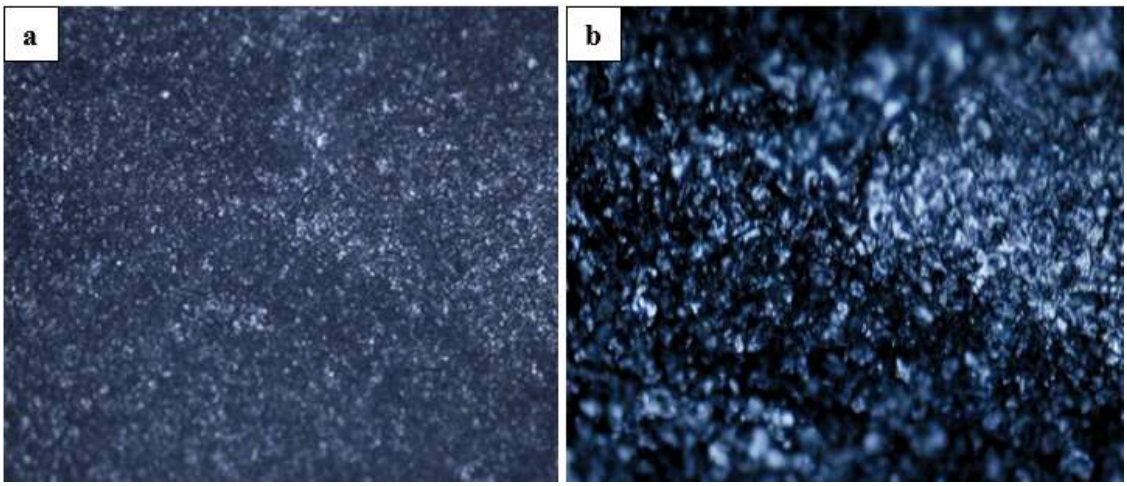

Figure 3: The OPM micrograph for sample AQ: a) 50x Magnification, b) 100x Magnification

Sample QQ has a highly polished and compact grain structure, especially at 100× magnification (Figure 4b), where the martensitic characteristics look more aligned and continuous compared to Q. The 50× image (Figure 4a) depicts a densely packed structure, likely indicating improved phase uniformity resulting from repeated thermal cycling. Nonetheless, certain evidence of structural banding or alignment is discernible, potentially signifying localized thermal stress or pre-existing grain boundaries affecting the martensitic transformation trajectory. The enhanced hardness in QQ corroborates this

refined microstructure; however, such homogeneous martensitic structures frequently demonstrate diminished corrosion resistance, as evidenced by subsequent electrochemical studies.

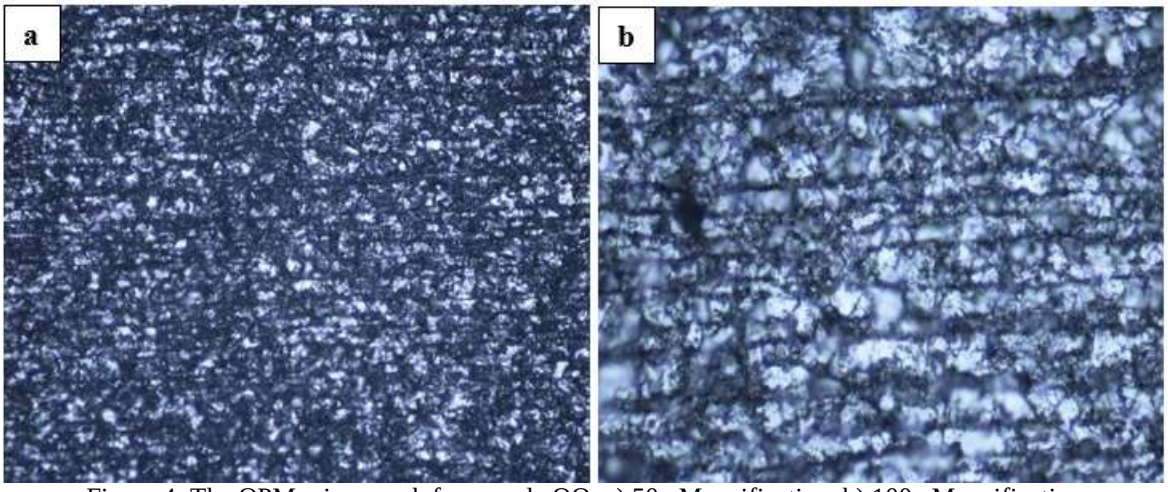

Figure 4: The OPM micrograph for sample QQ: a) 50x Magnification, b) 100x Magnification

These optical micrographs validate the anticipated transitions from ferrite–pearlite (A) to totally martensitic (Q), with AQ and QQ displaying intermediate and refined microstructures, respectively. The images correspond effectively with the mechanical and corrosion characteristics examined subsequently: the refined, uniform martensite in Q and QQ increases hardness, whilst the retained ferrite in A and AQ boosts ductility and corrosion resistance under specific conditions. These microstructural insights highlight the relationship among heat treatment, microstructure, and subsequent performance in acidic and marine environments.

3.2 Microhardness Properties of Heat-Treated Specimens

The microhardness characteristics of the heat-treated carbon steel specimens are summarized in Table 1 and further illustrated in Figures 5 and 6. These results demonstrate a clear dependence of surface hardness on the type and sequence of heat treatment applied, correlating directly with the underlying phase transformations and microstructural refinements induced during thermal processing.

Table 1: Microhardness property of the heat-treated specimens

Nomenclatures	Microhardness $HV_{0.3}$
Control	170
A	138
AQ	196
Q	404
QQ	224

As shown in Table 1, the control sample, which did not undergo any heat treatment, recorded a baseline microhardness of 170 $HV_{0.3}$. The normalized (A) specimen exhibited the lowest hardness among the heat-treated samples at 138 $HV_{0.3}$, reflecting the formation of a relatively soft ferrite–pearlite structure due to the slow cooling rate. In contrast, the quenched (Q) sample demonstrated the highest hardness, reaching 404 $HV_{0.3}$, which is attributable to the formation of a dense and hard martensitic structure resulting from rapid quenching. The AQ (normalized followed by quenching) and QQ (cyclic quenched) samples displayed intermediate hardness values of 196 $HV_{0.3}$ and 224 $HV_{0.3}$, respectively. These values suggest a mixed-phase microstructure in AQ, while the improved hardness in QQ is due to enhanced martensitic uniformity and transformation kinetics resulting from successive quenching cycles.

Figure 5 provides a pie chart that visually compares the hardness contributions of each sample relative to the entire dataset. The Q sample accounts for the largest proportion (35.7%) of the overall hardness distribution, significantly higher than all other samples, followed by QQ (19.8%), AQ (17.3%), Control (15%), and A (12.2%). This distribution underscores the effectiveness of quenching, especially in a single cycle, in maximizing hardness through phase transformation.

Further insights into the depth-dependent hardness distribution are provided in Figure 6. The microhardness profiles show that the A sample maintained a relatively flat and low hardness curve across the entire 3000 µm depth, consistent with a homogeneous and soft ferrite-pearlite matrix. In contrast, the Q and QQ samples exhibit significantly higher and more stable hardness profiles, with the QQ sample maintaining values above 400 $HV_{0.3}$ across most of the depth range.

This indicates a deep and uniform martensitic layer, which is beneficial for applications requiring surface wear resistance and mechanical durability. The AQ sample again presents an intermediate profile, with some variability in hardness along the depth, possibly due to partial transformation and microstructural heterogeneity introduced by sequential thermal cycling.

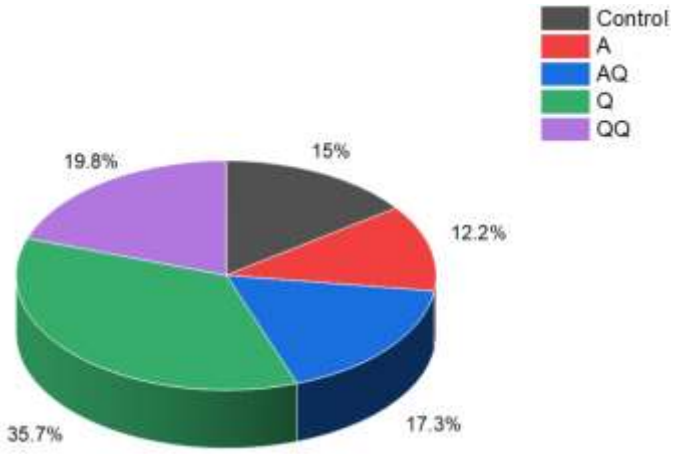

Figure 5: The graphical representation of the microhardness properties of the samples

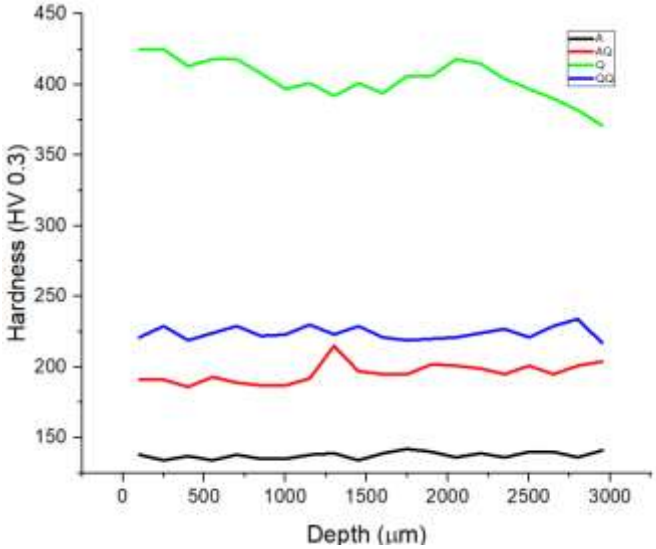

Figure 6: The microhardness profiles of the heat-treated samples

The significance of heat treatment design in tailoring the mechanical properties of carbon steel is evidenced by the correlation between surface and subsurface hardness measurements and the microstructural changes depicted in the optical micrographs. Quenching specifically produces a hard, martensitic surface; increased quenching in QQ improves uniformity but slightly reduces peak hardness, likely due to accumulated internal stress. The results validate that through thermal route management, the hardness of carbon steel may be effectively altered, hence providing a foundation for optimizing mechanical performance in applications subjected to abrasive wear or impact loading in corrosive environments.

3.2 Electrochemical Behavior of the Heat-Treated Specimens in an Acidic Environment

Linear polarization measurements were employed to assess the electrochemical corrosion performance of heat-treated carbon steel specimens in a simulated acidic solution, as demonstrated in Table 2 and Figure 7. The results highlight the influence of heat treatment on corrosion potential (ECORR), corrosion current density (ICORR), corrosion rate, and polarization resistance (RP), revealing distinct trends among the samples.

The AQ sample showed a slightly more negative ECORR (-0.6796 V) and a lower ICORR (2.14×10^{-7} A/cm²), accompanied by a reduced corrosion rate (0.024915 mm/year) and slightly decreased RP (37716 Ω·cm²). This suggests that the dual-phase microstructure formed in AQ provides modest corrosion protection, possibly due to refined martensite–ferrite interfaces offering better passive film adherence or reduced localized galvanic activity.

The Q sample (quenched) demonstrated the lowest ICORR (1.97×10^{-7} A/cm²) and corrosion rate (0.022883 mm/year), alongside a moderately high polarization resistance (43594 Ω·cm²). This indicates that the predominantly martensitic microstructure achieved through rapid quenching may confer some corrosion resistance in acidic media, likely due to its

higher dislocation density and finer grain structure, which can hinder corrosion propagation despite increased lattice distortion.

Table 2: Corrosion test data of the specimens in an acidic environment

Samples	E_{CORR}	I_{CORR}	Corrosion Rate (mm/yr)	Polarization Resistance (Ω/cm^2)
A	-0.6652	2.2423E-07	0.026055	45766
AQ	-0.67958	2.14E-07	0.024915	37716
Q	-0.67513	1.97E-07	0.022883	43594
QQ	-0.74599	3.77E-07	0.043861	32913

The normalized sample (A) exhibited the most positive corrosion potential (-0.6652 V) and the highest polarization resistance (45766 Ω·cm²), suggesting a relatively lower tendency for anodic dissolution and greater electrochemical stability. Despite this, its corrosion current density (2.24×10^{-7} A/cm²) and corrosion rate (0.026055 mm/year) were the highest among the single-step heat-treated samples, indicating that while passivation may be present, it is less effective in reducing active corrosion under acidic conditions.

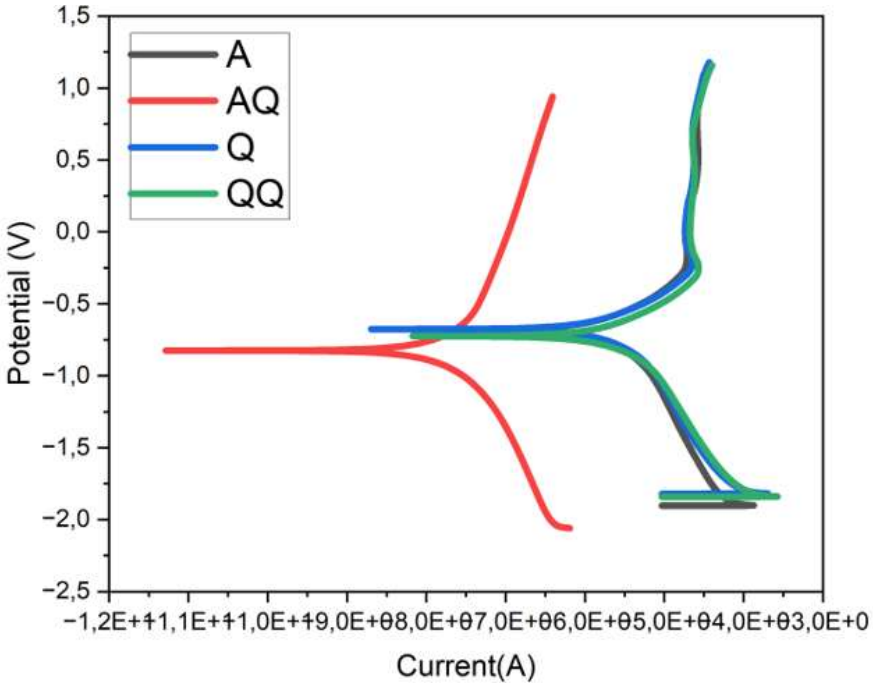

Figure 7: The linear polarization curve of the specimens in the acidic environment

In contrast, the QQ sample exhibited the most negative ECORR (-0.74599 V) and the highest ICORR (3.77×10^{-7} A/cm²), leading to the highest corrosion rate (0.043861 mm/year) and the lowest polarization resistance (32913 Ω·cm²) among all samples. These results clearly indicate that repeated quenching may introduce significant residual stresses, microstructural inhomogeneity, or surface imperfections that compromise corrosion resistance in aggressive acidic environments.

The polarization curves in Figure 7 reinforce these findings, with the AQ and Q curves displaying lower current densities over the potential range, while the QQ curve exhibits a steeper slope, reflecting accelerated anodic and cathodic reactions. Overall, the results show that while martensitic transformation (as in Q) can slightly improve corrosion resistance, excessive thermal cycling (as in QQ) is detrimental. The AQ condition offers a balanced compromise, although air cooling alone (A) still provides the most electrochemically stable potential, despite its limited passive protection.

3.3 Wear Performance of Heat-Treated Specimens

The wear behavior of the untreated and heat-treated carbon steel samples was evaluated under sliding conditions at two different applied loads: 10 N and 20 N. The results, as presented in Table 3 and illustrated in Figures 7 and 8, demonstrate a clear influence of heat treatment on wear resistance, which can be correlated with the observed microstructural modifications and hardness profiles.

At 10 N, the untreated control sample exhibited the highest wear rate at 1.166×10^{-3} mm³/N·m, indicating poor wear resistance due to its relatively low surface hardness and coarse ferrite–pearlite microstructure. The normalized (A) sample followed with a wear rate of 2.778×10^{-5} mm³/N·m, reflecting a marginal improvement owing to slight grain refinement.

In contrast, the quenched (Q) and AQ (normalized followed by quenching) samples recorded significantly lower wear rates of 8.486×10^{-7} mm³/N·m and 1.368×10^{-6} mm³/N·m, respectively, consistent with their martensitic and dual-phase structures that promote higher hardness and abrasion resistance. The cyclic quenched (QQ) specimen demonstrated the lowest wear rate at this load (3.901×10^{-6} mm³/N·m), indicating superior wear resistance likely due to its highly refined and uniformly distributed martensitic phase.

Table 3: The wear test results of the specimens

WEAR TEST OF THE CONTROL AND THE SAMPLE			
Samples	**LOAD**	**10 N (mm^3/N/m)**	**20 N (mm^3/N/m)**
Control		1.166E-03	1.72E-03
A		2.778E-05	1.064E-04
Q		8.486E-05	1.563E-07
AQ		1.368E-07	2.732E-05
QQ		3.901E-05	2.05E-07

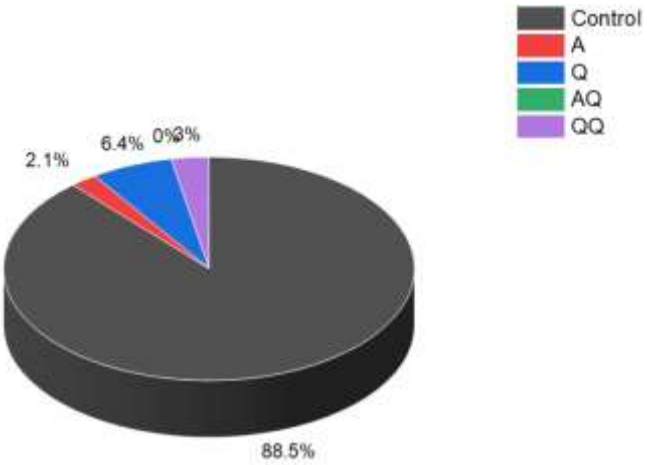

Figure 7: The wear rate of the specimens at 10 N.

This trend is further visualized in Figure 7, where the control sample overwhelmingly accounts for 88.5% of total wear volume under 10 N loading. All heat-treated samples collectively represent less than 12% of the wear volume, with QQ contributing just 0.3%, highlighting the effectiveness of heat treatment, particularly repeated quenching, in reducing material loss during frictional contact.

Under a higher load of 20 N, similar trends persist but with increased wear rates across all samples. The control sample again performed the worst, with a wear rate of 1.72×10^{-3} mm³/N·m, while the A sample recorded 1.064×10^{-4} mm³/N·m, suggesting that the wear performance of ferrite–pearlite structures deteriorates more severely under higher mechanical stress. The Q and AQ samples maintained relatively good performance, with wear rates of 1.563×10^{-7} mm³/N·m and 2.732×10^{-5} mm³/N·m, respectively. Notably, the QQ sample continued to show excellent resistance, with a wear rate of only 2.05×10^{-7} mm³/N·m, reaffirming its enhanced surface durability even under intensified loading.

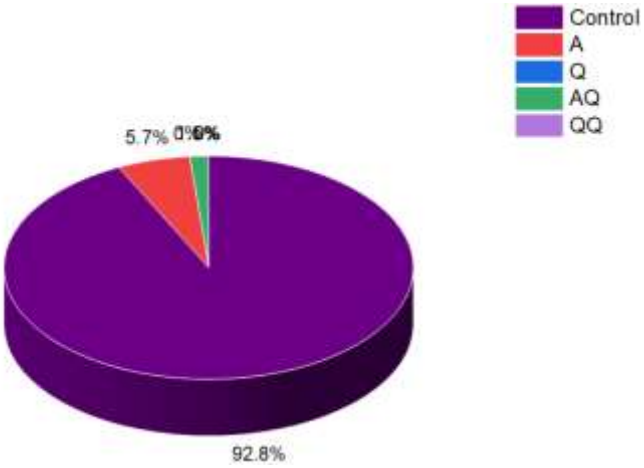

Figure 8: The wear rate of the specimens at 20 N.

As illustrated in Figure 8, at 20 N, the QQ sample accounts for just 0.2% of total wear, while the control sample dominates with 92.8%, and Q and AQ contribute 5.7% and 1.3%, respectively. These figures further validate the significant improvements in wear resistance achieved through controlled heat treatment and martensitic phase optimization.

Overall, the wear performance data align well with the hardness measurements, supporting the conclusion that increased hardness through quenching and refined martensitic transformation significantly enhances wear resistance. The exceptional performance of the QQ sample at both loads suggests that double quenching imparts a highly durable surface capable of withstanding mechanical degradation, making it a suitable treatment path for components operating under abrasive or high-load conditions.

4. CONCLUSION

This study demonstrates that heat treatment considerably influences the microstructure, corrosion resistance in acidic environments, and wear performance of low-carbon steel. The thermal history is critical in determining the mechanical and electrochemical properties of steel, as demonstrated by four distinct thermal processing methods: normalizing (A), water quenching (Q), normalized followed by quenching (AQ), and cyclic quenching (QQ).

Microstructural analyses revealed that normalizing produced a coarse ferrite–pearlite matrix characterized by low hardness yet moderate corrosion resistance. Cyclic quenching (QQ) enhanced the martensitic structure formed after quenching, improving wear resistance under various loads; nevertheless, it diminished corrosion resistance due to residual stresses and structural inhomogeneity. The dual-phase microstructure and reduced internal stress rendered the AQ condition the most balanced treatment, merging increased hardness with superior corrosion resistance in a sulfuric acid environment.

Wear tests under 10 N and 20 N loads revealed a significant relationship between hardness and wear resistance; the QQ sample had the lowest wear rates because of its hardened surface. On the other hand, the control and A samples, defined by reduced hardness, saw the most material loss. Whereas the QQ sample showed the most severe corrosion attack, Q and AQ treatments in H_2SO_4 demonstrated lower corrosion current density and improved polarization resistance.

This study underscores the necessity of tailoring heat treatment protocols to achieve an optimal equilibrium between corrosion resistance and mechanical durability. The AQ treatment provides an optimal balance of surface hardness, structural integrity, and environmental durability, making it recommended for components subjected to simultaneous acidic and abrasive conditions.

REFERENCES

[1] Alfirano, U. S. Eben, & Hidayat M. (2018). Microstructures and mechanical properties of duplex low carbon steel. *IOP Conference Series: Materials Science and Engineering*, 344(1), 012001, doi: 10.1088/1757-899X/344/1/012001.

[2] Singh A. K., Bhattacharya B., and Biswas S. (2024). High strength, ductility and sheet formability by normalizing and quenching of low carbon microalloyed dual-phase steel. *Materials Science and Engineering: A*, 890, 145848, doi: https://doi.org/10.1016/j.msea.2023.145848.

[3] Fu Y., Gao J., Pang Y., Tong W., & Zhang H. (2020). Surface nano-alloying treatment of low carbon steel. *Metallic Materials/Kovové Materiály*, 58(3).

[4] Paul S. (2015). Thermally Sprayed Corrosion Resistant Alloy Coatings on Carbon Steel for use in Supercritical CO2 Environments. in *CORROSION 2015*, All Days, NACE-2015-5939.

[5] Aramide B., Pityana S., Jamiru T., Popoola P., & Sadiku R. (2021). Influence of Vanadium-Chromium Carbide on the Microstructure of Reinforced FeCrV15 Hardfacing during Laser Cladding Deposit. *Journal of Materials Engineering and Performance*, doi: 10.1007/s11665-021-06153-w.

[6] Aramide B., Pityana S., Sadiku R., Jamiru T., & Popoola P. (2021). Improving the durability of tillage tools through surface modification—a review. *The International Journal of Advanced Manufacturing Technology*, 116(1), 83-98, doi: 10.1007/s00170-021-07487-4.

[7] Podaný P., Studecký T., & Kocijan A. (2023). Material Properties of High-strength High Chromium TWIP Steel with Increased Corrosion Resistance. *Manufacturing Technology Journal*, journal article, 23(2), 241-246, doi: 10.21062/mft.2023.025.

[8] Aramide B., Popoola P., Sadiku R., Jamiru T., & Pityana S. (2021) Influence of extra chromium addition on the microstructure, hardness, and corrosion behaviour of high carbon ferrochrome FeCrV15 deposited through laser cladding on steel baseplate for tillage application. *Surface Topography: Metrology and Properties*, 9(4), 045029, doi: 10.1088/2051-672x/ac314f.

[9] Puspitasari P., Alifian C., Aripriharta A., Razak J. A., & Pratama M. M. A. (2020). Corrosion Resistance Analysis of ST37 Carbon Steel Material Using Phosphate Conversion Coating in Various Immersion Durations. *Key Engineering Materials*: Trans Tech Publ, 851, 61-67.

[10] Krishna N. G., Thinaharan C., George R. P., Parvathavarthini N., & Kamachi Mudali U. (2015). Surface modification of type 304 stainless steel with duplex coatings for corrosion resistance in sea water environments, *Surface Engineering*, 31(1), 39-47, doi: 10.1179/1743294414y.0000000354.

[11] Aramide B., Sadiku R., Popoola P., Pityana S., & Jamiru T. (2022). Effect of powder flowrate on the microstructure of FeCrV15 clad, developed via the laser cladding technique. *Materials Today: Proceedings*.

[12] Aramide B., Sadiku R., Popoola P., Pityana S., & Jamiru T. (2022). The microstructure and anti-wear property of FeCrV15 and FeCrV15+Cr deposits fabricated via laser deposition on steel base-plate for soil-working tools. *Applied Physics A*, 128(6), 490, doi: 10.1007/s00339-022-05632-8.
[13] Herbst S., Schledorn M., Maier H. J., Milenin A., & Nürnberger F. (2016). Process Integrated Heat Treatment of a Microalloyed Medium Carbon Steel: Microstructure and Mechanical Properties. *Journal of Materials Engineering and Performance*, 25(4), 1453-1462, doi: 10.1007/s11665-016-2004-9.
[14] Zhao X., Zhang, X., Zhou, J., Chen, Y., Zhang, F., Zhang, J., & Yan, Q. (2025). Direct quenching and double tempering obtain high strength and toughness of Cu-bearing HSLC martensitic steel. *Journal of Materials Research and Technology*, 35, 13-24, doi: https://doi.org/10.1016/j.jmrt.2025.01.006.
[15] Zhou X., Zhao W., Dong L., & Song N. (2022). Effect of Quenching and Tempering Temperatures on Microstructure and Properties of Ultrahigh Strength Cast Steel. *Steel Research International*, 93(11), 2200328, doi: https://doi.org/10.1002/srin.202200328.
[16] Branco R., & Berto F. (2018). Mechanical Behavior of High-Strength, Low-Alloy Steels. *Metals*, 8(8), 610, [Online]. Available: https://www.mdpi.com/2075-4701/8/8/610.
[17] Singh R., Joshi A., & Rani S. (2025). Transforming Sustainable Business Models for Manufacturing Industry to Build Zero Carbon Industry in *Zero Carbon Industry, Eco-Innovation and Environmental Sustainability*, Singh R., Joshi A., Filho W. L., & Khan S. Eds. Cham: Springer Nature Switzerland, 3-19.
[18] Colla V., & Branca T. A. (2021). Sustainable Steel Industry: Energy and Resource Efficiency, Low-Emissions and Carbon-Lean Production. *Metals*, 11(9), 1469. [Online]. Available: https://www.mdpi.com/2075-4701/11/9/1469.
[19] Yu W. W., LaBoube R. A., & Chen H. (2019). *Cold-formed steel design*. John Wiley & Sons.
[20] Aramide B. P., Jamiru T., Adegbola T. A., Popoola A. P. I., & Sadiku E. R. (2024) "Influence of TiB2 Incorporation on Microstructural Evolution in Laser-Clad FeCrV15 + TiB2 Deposits. *Journal of Materials Engineering and Performance*, doi: 10.1007/s11665-024-09618-w.